Frontiers of Physics
https://doi.org/10.1007/s11467-021-1092-7
Front. Phys.
17(1), 12501 (2022)

RESEARCH ARTICLE

Multiphonon-resonance quantum Rabi model and adiabatic passage in a cavity-optomechanical system

Zhi-Rong Zhong†, Lei Chen, Jian-Qi Sheng, Li-Tuo Shen, Shi-Biao Zheng

Fujian Key Laboratory of Quantum Information and Quantum Optics, College of Physics and Information Engineering, Fuzhou University, Fuzhou 350108, China
Corresponding author. E-mail: †zhirz@fzu.edu.cn
Received March 8, 2021; accepted June 2, 2021

In this paper, we propose a scheme to achieve a multiphonon-resonance quantum Rabi model and adiabatic passage in a strong-coupling cavity optomechanical system. In the scheme, when the driving bichromatic laser beam is adjusted to the off-resonant j-order red- and blue-sideband, the interaction between the cavity and mechanical oscillator leads to a j-phonon resonance quantum Rabi model. Moreover, we show that there exists a resonant multi-phonon coupling via intermediate states connected by counter-rotating processes when the frequency of the simulated bosonic mode is near a fraction of the transition frequency of the simulated two-level system. As a typical example, we theoretically analyze the two-phonon resonance quantum Rabi model, and derive an effective Hamiltonian of the six-phonon coupling. Finally, we present a method of six-phonon generation based on adiabatic passage across the resonance. Numerical simulations confirm the validity of the proposed scheme. Theoretically, the proposed scheme can be extended to the realization of $3j$-phonon state.

Keywords quantum Rabi model, cavity-optomechanical system, adiabatic passage

1 Introduction

The quantum Rabi model (QRM) [1], which describes the dipolar coupling between a two-level system and a quantized bosonic field, has played an important role in quantum optics and condensed matter systems for the last few decades. The QRM requires to take the counter-rotating term into account in the interaction Hamiltonian that is neglected in the Jaynes–Cummings model (JCM), which is a solvable system where the rotating-wave approximation (RWA) is applied. Under RWA, this system can exhibit various quantum effects, such as quantum Rabi oscillations [1] and anti-Zeno effect [2, 3]. Typically, the RWA is valid when and only when the coupling strength is small enough. With the recent advances in quantum technology, in several systems, the coupling strength has been extended to the ultrastrong coupling (USC) [4, 5] and deep strong coupling (DSC) regimes [6–8], which indicated that the RWA is no longer valid. In recent years, a variety of interesting results have been investigated in the QRM, such as quantum vacuum radiation [9, 10], Quantum phase transition and quench dynamics [11], superradiance transition [12], collapse and revival dynamics in the deep strong coupling regime [6], and scalable quantum memory [13]. Noted that several proposals and experimental realizations of the QRM in different quantum system have been put forward, such as optical lattices [14], circuit QED [15], as well as trapped ions [16, 17].

In QRM, one interesting feature is that when considering the counter-rotating terms, the number of excitations in the cavity-emitter system is no longer conserved, and the virtual transitions should not be excluded. Thus, the higher order resonant transitions via intermediate states will occur. A recent research shows that a resonant three-photon coupling can be achieved when the frequency of the cavity field is near one-third of the atomic transition frequency [18]. Moreover, it is shown that a system consisting of a single qubit ultrastrongly coupled to a resonator can exhibit anomalous vacuum Rabi oscillations where two or three photons are jointly emitted by the qubit into the resonator and reabsorbed by the qubit in a reversible and coherent process [19].

Cavity-optomechanical system [20], where a cavity field couples to a mechanical oscillator via the radiation-pressure force interaction, is a promising venue to realize quantum entanglement and quantum information processing in the mesoscopic field. Based on this system, schemes for entanglement generation [20–29] and high-precision measurements [30, 31], as well as quantum interfaces [32–34] have been put forward. On the other hand, theoretical studies on cavity-optomechanical system had

* This article can also be found at http://journal.hep.com.cn/fop/EN/10.1007/s11467-021-1092-7.

been focused on the single-photon strong coupling regime, in which the radiation pressure of a single photon can produce observable effects and a strong photon nonlinearity, such as photon blockade effect [35–45]. Although great progress has been made in the theoretical study of the optomechanical system, the realization of QRM of this system remains a challenge [46, 47]. The main obstacle to achieve the QRM is that it is difficult to choice the actors of qubit in cavity-optomechanical system.

In this paper, we show that the multiphonon resonance QRM and adiabatic passage can be realized in a cavity optomechanical system. Our proposal focuses on the single-photon strong-coupling regime. In the scheme, with suitable setting of parameters of the driving laser, the dynamics of the system can be treated as the multiphonon resonance QRM between the simulated two-level system and the simulated bosonic mode. In addition, we also show that this resonance QRM can be exploited to generate multiphonon states through adiabatic passage. As a typical example, we theoretically analyze the two-phonon resonance QRM, and show the generation of six-phonon states through adiabatic passage by using this two-phonon resonance QRM. Numerical simulations show that the proposed scheme is available. In principle, this scheme can be used to prepare $3j$-phonon state in cavity optomechanical system.

Our work is organized as follows. In Section 2, we present the theoretical model, and show that the interaction between the cavity and the mechanical oscillator can be treated as a multiphonon resonance QRM by suitably adjusting the detuning of the driving laser. Also, we discuss the nature of energy eigenvectors across the resonance and analyze the position of the resonance from the effective Hamiltonian. In Section 3, we discuss a scheme for six-phonon generation via adiabatic passage and present numerical simulations of the fidelities of the target state. Then, a wigner function of targeted state is numerically simulated and is compared to that of the ideal six-phonon state. A brief discussion of the experimental feasibility and summary appear in Section 4.

2 Theoretical model and numerically simulation

Our proposal is based on a single-mode cavity with a movable perfectly-reflecting microsize mirror (treated as mechanical oscillator). Also, the cavity mode couples to the mechanical oscillators through the radiation-pressure interaction induced by a driving bichromatic laser. It is necessary to point out that the bichromatic laser has been successfully used for different purposes in trapped ion system [48–50]. The total Hamiltonian of this system can be expressed in the form ($\hbar = 1$)

$$H = H_0 + H_{\rm OM} + H_{\rm D}, \tag{1}$$

where

$$H_0 = \omega_c a^\dagger a + \omega_m b^\dagger b \tag{2}$$

is the free Hamiltonian,

$$H_{\rm OM} = g_0 a^\dagger a (b^\dagger + b) \tag{3}$$

is the standard optomechanical Hamiltonian, and

$$H_{\rm D} = \sum_{d=l,r} \Omega\{a^\dagger \exp[-{\rm i}(\omega_d t + \phi_d)] + {\rm H.c}\}, \tag{4}$$

is the the laser driven term. Here a ($a^\dagger$) is the annihilation (creation) operator for the cavity, and b ($b^\dagger$) is the annihilation (creation) operator for the mechanical oscillator. The parameters ω_c and ω_m are the frequencies of the cavity and the mechanical oscillator, while the other parameters Ω, ω_d, and ϕ_d ($d = l, r$) are the Rabi frequency, frequency and initial phase of the driving laser field, respectively. In addition, $g_0 = \omega_c x_{\rm zpf}/L$ is the single-photon optomechanical coupling strength, where $x_{\rm zpf} = \sqrt{1/(2M\omega_m)}$ is the zero-point fluctuation of the moving mirror with mass M, and L is the length of the cavity.

To solve the Hamiltonian H, we firstly apply a unitary transformation $V_1 = \exp\left[(g_0/\omega_m)a^\dagger a(b^\dagger - b)\right]$ to transform the Hamiltonian H to $H_1 = V_1 H V_1^\dagger$. Thus, we obtain a new Hamiltonian

$$H_1 = (\omega_c - \Delta_0 a^\dagger a)a^\dagger a + \omega_m b^\dagger b + \sum_{d=l,r} \Omega\left[a^\dagger {\rm e}^{-{\rm i}(\omega_d t + \Phi_d)} {\rm e}^{\eta(b^\dagger - b)} + {\rm H.c}\right], \tag{5}$$

where $\Delta_0 = g_0^2/\omega_m$ characterizes the nonlinearity of the cavity field induced by mechanical oscillators, and the parameter $\eta = g_0/\omega_m$ can be treated as the Lamb-Dicke parameter similar to that used in the analysis of trapped ions [16, 17]. In the scheme, we consider the strong optomechanical coupling, which guarantees a big nonlinear parameter Δ_0 so that the photon blockade can occur [43, 51]. In this case, the cavity field is reduced to the two lowest-energy levels, $|0\rangle$ and $|1\rangle$. Then we can rewrite the creation operator of the cavity field as $a^\dagger = |1\rangle\langle 0| = \sigma_+$, and further introduce a new operator $\sigma_z = |1\rangle\langle 1| - |0\rangle\langle 0|$. Thus, the Hamiltonian H_1 can be rewritten as

$$H_2 = H_0^1 + H_I^{'}, \tag{6}$$

where

$$H_0^1 = \frac{\omega_0}{2}\sigma_z + \omega_m b^\dagger b, \tag{7}$$

and

$$H_I^{'} = \sum_{d=l,r} \Omega\sigma_+ {\rm e}^{-{\rm i}(\omega_d t + \Phi_d)} \exp\left[\eta(b^\dagger - b)\right] + {\rm H.c.}$$

$$= \sum_{d=l,r} \Omega\sigma_+ \mathrm{e}^{\frac{-\eta^2}{2}} \mathrm{e}^{-\mathrm{i}(\omega_d t+\Phi_d)} \sum_{m,n} \frac{\eta^{(m+n)}}{m!n!} b^{\dagger m} b^n + \mathrm{H.c.} \tag{8}$$

Here, $\omega_0 = \omega_c - \Delta_0$. In the interaction picture, with $H_I = \mathrm{e}^{\mathrm{i}H_0^1 t} H_I' \mathrm{e}^{-\mathrm{i}H_0^1 t}$, we have a new Hamiltonian, which reads

$$H_I = \Omega\sigma_+ \mathrm{e}^{\frac{-\eta^2}{2}} \sum_{m,n} \sum_{d=l,r} \mathrm{e}^{-\mathrm{i}\Phi_d} \mathrm{e}^{-\mathrm{i}(\omega_d-\omega_0)t} \frac{\eta^{(m+n)}}{m!n!} \times b^{\dagger m} b^n \mathrm{e}^{\mathrm{i}(m-n)\omega_m t} + \mathrm{H.c.} \tag{9}$$

We here consider the case where the laser is adjusted to the off-resonant j-order red- and blue-sideband excitations, with corresponding detunings are δ_r and δ_b, respectively, i.e., $\omega_b = \omega_0 - j\omega_m + \delta_r$, and $\omega_r = \omega_0 + j\omega_m + \delta_b$. In this case, the interaction Hamiltonian for such a system is

$$H_I^j = \lambda\sigma_+ (b^{\dagger j} \mathrm{e}^{-\mathrm{i}\delta_r t} + b^j \mathrm{e}^{-\mathrm{i}\delta_b t}) + \mathrm{H.c.}, \tag{10}$$

where $\lambda = \Omega f_j(\widehat{n})$ is the effective coupling strength, which is modulated by the nonlinear parameter η and nonlinear function $f_j(\widehat{n})$ [52],

$$f_j(\widehat{n}) = \mathrm{e}^{-\frac{\eta^2}{2}} \sum_m \frac{(\mathrm{i}\eta)^{2m}}{m!(m+j)!} b^{\dagger m} b^m, \tag{11}$$

with $n = m + j$ and $b^{\dagger m} b^m = \frac{n!}{(n-m)!}$. Here, the initial phase Φ_d $(d = l, r)$ are set to zero. The above Hamiltonian (10) corresponds to the interaction picture Hamiltonian of j-phonon quantum Rabi model with respect to the free Hamiltonian $H_0 = \frac{1}{4}(\delta_r + \delta_b)\sigma_z + \frac{1}{2j}(\delta_r - \delta_b) b^\dagger b$. Therefore, after applying an undoing transformation to Hamiltonian (10), we have

$$H_R^j = \omega_0^R \frac{\sigma_z}{2} + \omega^R b^\dagger b + \lambda(b^{\dagger j} + b^j)(\sigma^+ + \sigma^-), \tag{12}$$

where $\omega_0^R = -\frac{1}{2}(\delta_r + \delta_b)$ and $\omega^R = \frac{1}{2j}(\delta_r - \delta_b)$ represent the qubit transition frequency of the simulated two-level system and the frequency of the simulated bosonic mode, respectively. Next, we focus on the situation where the frequency detuning between the simulated two-level system and the simulated bosonic mode is large. Specifically, if we consider the condition $\omega_0^R \simeq 3j\omega^R$, and the corresponding detuning $\Delta = \frac{3j-1}{3j}\omega_0^R \gg \lambda$. Under this parameter region, if the simulated two-level system is prepared in the excited state $|e\rangle$ and the simulated bosonic mode is in the vacuum state $|0\rangle$, i.e, $|e, 0\rangle$. According to the Hamiltonian (12), the term of RWA makes the system evolve to state $|g, j\rangle$, while the counter-rotating terms would enable a virtual transition from $|g, j\rangle$ to $|e, 2j\rangle$, and subsequently the system can evolve to the final state $|g, 3j\rangle$. Since $\omega_0^R \simeq 3j\omega^R$, thus $|g, j\rangle$ and $|e, 2j\rangle$ are the intermediate states, while $|e, 0\rangle$ and $|g, 3j\rangle$ can resonantly coupled with each other.

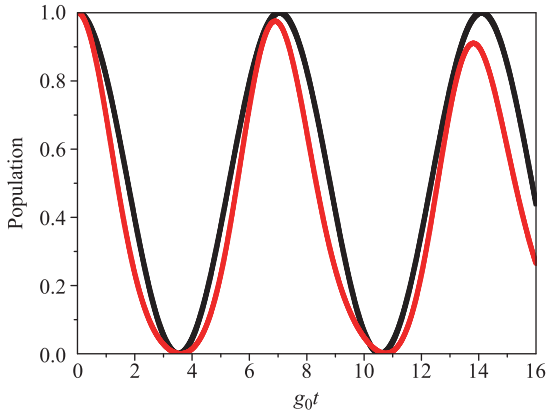

Fig. 1 Time evolution of the population governed respectively by the effective Hamiltonian (black curve) and the full Hamiltonian (red curve).

In order to confirm the validity of all our above derivations, we numerically simulate the dynamics governed by the effective model in Eq. (12) and compare it to the dynamics governed by the full Hamiltonian in Eq. (1). We set the parameters as: $j = 2$, $\omega_m = 0.1\omega_c$, $\Omega = 0.3\omega_c$ and $g_0 = 1.6\omega_m$. In Fig. 1, the red curve describes the time evolution of the population of state $|0, 0\rangle$ (the cavity mode and the mechanical oscillator are all in the vacuum states) governed by full Hamiltonians (1), while the black curve describes time evolution of the population of state $|e, 0\rangle$ (the simulated two-level system is initially in the excited state and the simulated bosonic mode are all in the vacuum states) governed by the effective Hamiltonians (12). It is obvious that the approximations adopted when deriving the effective Hamiltonian (12) are valid, since the two curves described by the full and effective Hamiltonians nearly coincide.

On the other hand, in an isolated system, the radiation pressure force applied to the oscillator is proportional to the photon number n_c and thereby lowers the energy of this photon state by $n_c \times g_0^2/\omega_m$ and leads to different resonance conditions for the first and the second laser photons exciting the cavity under the strong single-photon coupling coefficient g_0. Thus, if the driving laser is on resonance with the $|0\rangle \to |1\rangle$ transition, i.e., $\omega_c - \omega_m + g_0^2/\omega_m = 0$, the transition $|1\rangle \to |2\rangle$ is detuned by $2 \times g_0^2/\omega_m$ and will be suppressed because of under the large detuning condition $2 \times g_0^2/\omega_m \gg 1$. Thus, under this condition, the photon number in the cavity reduces to the two lowest-energy levels, $|0\rangle$ and $|1\rangle$. To make our analysis more convincing, we use Hamiltonian (1) to plot the photon number in the cavity, as is shown in Fig. 2. Figure 2 shows that the occupation probability of photon number states $|0\rangle$, $|1\rangle$, $|2\rangle$, $|3\rangle$, $|4\rangle$, $|5\rangle$, $|6\rangle$, $|7\rangle$ in the cavity are 0.581, 0.385, 0.031, 0.002, 0.0003, 0, 0 and 0, respectively. It shows that the probability of state $|2\rangle$ is smaller than that of states $|0\rangle$ and $|1\rangle$, and thus the system can be approximately confined in the subspace $\{|0\rangle, |1\rangle\}$.

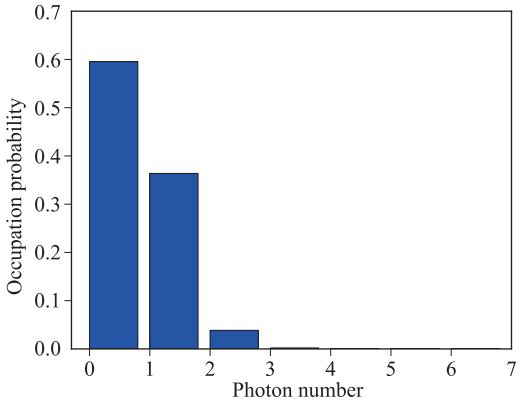

Fig. 2 The photon number in the cavity. The parameters are set as $\omega_c - \omega_m + g_0^2/\omega_m = 0$, $\Omega = 0.3g_0$, and $g_0/\omega_m = 0.43$. Here, the number of cavity photon is truncated at 7.

To make this physical process more clear, we now consider the condition that $j = 2$, and the corresponding Hamiltonian is

$$H_I^2 = \Omega[f_2(\widehat{n})b^2\sigma^+ e^{-i\delta_r t} + f_2(\widehat{n})b^{\dagger 2}\sigma^+ e^{-i\delta_b t}] + \text{H.c}, \quad (13)$$

where $f_2(\widehat{n})$ is introduced in Eq. (12). The Hamiltonian (13) corresponds to an interaction picture Hamiltonian of the two-phonon quantum Rabi model with respect to the free Hamiltonian $H_0 = \frac{1}{4}(\delta_r + \delta_b)\sigma_z + \frac{1}{4}(\delta_r - \delta_b)b^\dagger b$. Therefore, after applying an undoing transformation to Hamiltonian (13), we have

$$H_R^2 = \omega_0^R \frac{\sigma_z}{2} + \omega^R b^\dagger b + g(b^{\dagger 2} + b^2)(\sigma^+ + \sigma^-), \quad (14)$$

where $\omega_0^R = -\frac{1}{4}(\delta_r + \delta_b)$ and $\omega^R = \frac{1}{4}(\delta_r - \delta_b)$ represent the qubit transition frequency of the simulated two-level system and the frequency of the simulated bosonic mode, respectively, and $g = \Omega f_2(\widehat{n})$ is the coupling strength between them. Since the frequency ω_0^R is six times of the frequency ω^R, and the corresponding detuning is $\Delta = \frac{5}{6}\omega_0^R \gg g$, thus, the Hamiltonian in Eq. (14) represents a off-resonant two-phonon QRM. Under this parameter region, if the system is initially in the state $|e,0\rangle$, according to the Hamiltonian (14), the term of RWA makes the system evolve to state $|g,2\rangle$, while the counter-rotating terms would enable a virtual transition from state $|g,2\rangle$ to state $|e,4\rangle$, and subsequently the system can evolve to the final state $|g,6\rangle$. Because of the large detuning interaction, the states $|g,2\rangle$ and $|e,4\rangle$ are the intermediate states, while $|e,0\rangle$ and $|g,6\rangle$ can resonantly coupled with each other. The corresponding transitions are depicted in Fig. 3. In the figure, the excitation-number conserving and nonconserving process are represented by the arrowed red-solid and blue-dashed lines, respectively, while the green-dashed line represented the resonant coupling between the states $|e,0\rangle$ and $|g,6\rangle$. The parameters $\sqrt{2}g$, $\sqrt{12}g$, and $\sqrt{30}g$ are the corresponding transition matrix elements.

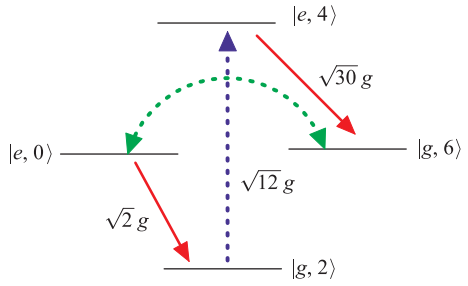

Fig. 3 Coupling between bare states $|e,0\rangle$, and $|g,6\rangle$ via intermediate states $|g,2\rangle$, and $|e,4\rangle$. Here, excitation number nonconserving process is represented by the arrowed blue-dashed line; $\sqrt{2}g$, $\sqrt{12}g$, and $\sqrt{30}g$ are the transition matrix elements.

In order to further illustrate the above analysis, we find out the energy spectrum as a function of ω^R/ω_0^R with $g = 0.06\omega_0^R$ under the large detuning condition based on the time-independent Schrodinger equation $H_R^2|\Psi_n\rangle = E_n|\Psi_n\rangle$, with $n = 1,2,3,4$. For simplicity, the effective coupling coefficient is set as a constant in the numerical simulation. When consider a more realistic situation, the effective coupling coefficient is not a constant, thus the Hamiltonian (13) can be considered as a nonlinear quantum Rabi model. Although the nonlinear term $f_2(\widehat{n})$ will suppress the collapses and revivals for a large Fock state $|n\rangle$ whenever $f_2(\widehat{n})|n\rangle = 0$ (i.e., $n = 17$), it is still can be applied to generate n-phonon state [49]. The result of numerical simulation is shown in Fig. 4. Here, Fig. 4(b) is the enlarged view of the spectrum delimited by a dotted square frame in Fig. 4(a). As seen from Fig. 4(b), at $\omega^R = 0.168\omega_0^R$, the two energy levels exhibit an avoided crossing, which serves as a signature of a resonance. At the avoided crossing point, the frequency of the simulated bosonic mode is equal to one- sixth of the frequency of the simulated two-level system. When the frequency of simulated bosonic mode across the avoided crossing point, the major component of $|\Psi_3\rangle$ changes from state $|e,0\rangle$ to state $|g,6\rangle$. While for state $|\Psi_4\rangle$, the trend of variety is the reversed, which indicates that the components of the two eigenvectors are exchanged across the resonance. Obviously, this avoided crossing corresponds to a six-phonon resonant coupling between the state $|e,0\rangle$ and $|g,6\rangle$, while such a resonant coupling does not appear in the traditional Jaynes–Cummings model. In this resonant two-phonon Rabi model, at the avoided crossing point, the states $|\Psi_3\rangle$ and $|\Psi_4\rangle$ can be approximated as the superposition state of $|e,0\rangle$ and $|g,6\rangle$, such as $\frac{1}{\sqrt{2}}(|e,0\rangle + |g,6\rangle)$ and $\frac{1}{\sqrt{2}}(|e,0\rangle - |g,6\rangle)$, respectively.

To investigate the effective coupling analytically, we start by reducing the Hamiltonian in the truncated Hilbert space spanned by the bare states $|e,0\rangle$, $|g,2\rangle$, $|e,4\rangle$, $|g,6\rangle$ and $|e,8\rangle$. As the parameters we used before, the detuning Δ is larger than the coupling strength g, thus, the above bare states are nearly decoupled from states outside the

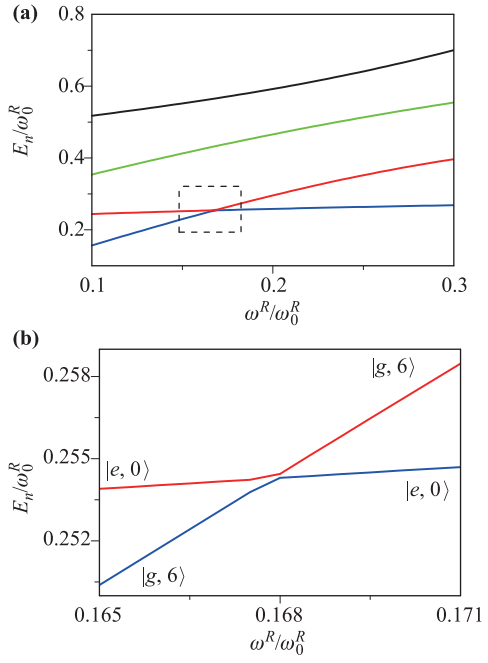

Fig. 4 **(a)** The energy spectrum as a function of ω^R/ω_0^R with $g = 0.06\omega_0^R$. **(b)** Enlarged view of the spectrum delimited by a dotted square frame in Fig. 2(a). This shows that the field frequency for the six-phonon resonance is given by $\omega^R = 0.168\omega_0^R$, at which the energy levels exhibit an avoided crossing.

truncated Hilbert space. The matrix form of the reduced Hamiltonian is given by

$$\begin{pmatrix} \frac{\omega_0^R}{2} & \sqrt{2}g & 0 & 0 & 0 \\ \sqrt{2}g & 2\frac{\omega_0^R}{2}-\frac{\omega_0^R}{2} & \sqrt{12}g & 0 & 0 \\ 0 & \sqrt{12}g & 4\frac{\omega_0^R}{2}+\frac{\omega_0^R}{2} & \sqrt{30}g & 0 \\ 0 & 0 & \sqrt{30}g & 6\frac{\omega_0^R}{2}-\frac{\omega_0^R}{2} & \sqrt{56}g \\ 0 & 0 & 0 & \sqrt{56}g & 8\frac{\omega_0^R}{2}+\frac{\omega_0^R}{2} \end{pmatrix}. \quad (15)$$

Here, the order of the column (row) is $|e,0\rangle$, $|g,2\rangle$, $|e,4\rangle$, $|g,6\rangle$ and $|e,8\rangle$. We have included state $|e,8\rangle$ to contributes to the Stark shift in the energy level for $|g,6\rangle$. In the six-phonon resonance, both $|g,2\rangle$ and $|e,4\rangle$ are the intermediate states which can be adiabatically eliminated. Thus, the effective Hamiltonian which describes a six-phonon coupling between the states $|e,0\rangle$ and $|g,6\rangle$ is

$$\begin{aligned} H_{\text{eff}} = &(\frac{\omega_0^R}{2} + 2\frac{g^2}{\Delta})\,|e,0\rangle\langle e,0| \\ &+ (6\omega^R - \frac{\omega_0^R}{2} - 36\frac{g^2}{\omega_0^R} - 56\frac{g^2}{5\omega^R})\,|g,6\rangle\langle g,6| \\ &+ \Omega_{\text{eff}}(|e,0\rangle\langle g,6| + \text{H.c.}). \end{aligned} \quad (16)$$

In the above effective Hamiltonian, the first two terms describe the Stark-shift of the states $|e,0\rangle$ and $|g,6\rangle$, respectively, while the last term describes the effective six-phonon coupling between these two states, with the corresponding coupling strength is $\Omega_{\text{eff}} = 72\sqrt{5}g^3/5(\omega_0^R)^2$.

3 Six-phonon generation based on adiabatic passage across the resonance

In this section, we will show the six-phonon state generation by slowly sweeping the vibration mode frequency across the resonance. Initially, suppose the system is prepared in the state $|e,0\rangle$, then the system would remain in this state when ω^R is far away from the resonant frequency $6\omega_0^R$. Subsequently, we adiabatically increase the bosonic mode frequency $\omega^R(t)$, after passing through the resonant frequency, a large population in state $|g,6\rangle$ can be obtained, which means that six-phonon state can be generated.

To verify the validity of the above adiabatic passage process, we perform a numerical simulation of the fidelity of the $|\Psi(t)\rangle$ with respect to the target state and the expectation value of the phonon number of the simulated bosonic mode. Noted that the adiabatic passage, has the advantage that it is insensitive to moderate fluctuations of experimental parameters [53–55]. Thus, it is considered as a powerful tool to manipulate quantum systems which has enjoyed widespread applications in many fields across quantum physics and in nonclassical state generation, i.e., has been used to create photon states [56–58] and kinds of entangled state [53, 54, 59–61]. With the coupling between the vibrational modes and the reservoir being included, the master equation at zero temperature is [9, 62]

$$\begin{aligned} \frac{\mathrm{d}\rho}{\mathrm{d}t} = &-\mathrm{i}\left[H_R^2(t),\ \rho\right] + \frac{\Gamma}{2}\left(2\sigma^-\rho\sigma^+ - \sigma^+\sigma^-\rho - \rho\sigma^+\sigma^-\right) \\ &+ \frac{\gamma_m}{2}\left(2b\rho b^\dagger - b^\dagger b\rho - \rho b^\dagger b\right), \end{aligned} \quad (17)$$

where Γ and γ_m are the decaying rates of stimulated two-level system and stimulated bosonic mode, respectively. The Hamiltonian $H_R^2(t)$ described as

$$H_R^2(t) = \omega_0^R\frac{\sigma_z}{2} + \omega^R(t)b^\dagger b + g(b^{\dagger 2} + b^2)(\sigma^+ - \sigma^-), \quad (18)$$

where $\omega^R(t)$ is time dependent and in the form

$$\omega^R(t) = \omega^R(0) + v_c t, \quad 0 \le t \le t_f, \quad (19)$$

here v_c serves as the sweeping speed, and controls the adiabaticity of the process. Thus, in a certain time, $\omega^R(t)$ can sweep across the resonance frequency, which indicates that the Hamiltonian in Eq. (18) is the same as that in Eq. (14). We set $g = 0.06\omega_0^R$, $v_c = 10^{-6}\omega_0^{R2}$, $\omega^R = 0.168\omega_0^R$, and $\Gamma = \gamma_m = 0.0005g$. Figure 5(a) shows the fidelity of the states $|\psi_\pm\rangle$, defined as $F = \langle\psi_\pm|\,\rho\,|\psi_\pm\rangle$, as a function of the evolution time, where ρ is the density operator of the system, $|\psi_+\rangle = |e,0\rangle$, and $|\psi_-\rangle = |g,6\rangle$, respectively. The numerical result shows that the fidelity of state $|g,6\rangle$ approaches $F \simeq 0.937$, and at the same time the fidelity of state $|e,0\rangle$ is 0. The deviation of the fidelity of state $|g,6\rangle$

is understood because the states $|e,4\rangle$ and $|e,8\rangle$ have a low but nonzero probability, although it's very small enough compared with that of state $|g,6\rangle$. In Fig. 5(b), we display numerical simulation of the expectation value of the phonon number $\langle b^\dagger b\rangle$, which also indicates the six-phonon generation. Noted that the six-phonon state is known as a nonclassical state and exist quantum interference features in phase space, also, has practical applications in quantum phononics, including the phonon lasers [63–68], phononic quantum networks [69, 70], quantum acoustic devices [71, 72] and ultrasensitive biodetection [73]. Noted that proposed proposal focus on the generation of multi-phonon states, offering the possibility for realizing pulsed phonon laser and single phonon source. In contrast, the previous schemes dealt with implementation of continuous output phonon laser [63–68]. Schemes have been proposed to generate multi-phonon state in a micromechanical oscillator [74], in a superconducting quantum interference device [75], in a bulk acoustic-wave resonator [76], in trapped ion [77], and in quantum dot system [78].

To further demonstrate the production of the desired six-phonon state, we now perform the full Wigner tomography at the time $gt \simeq 1.1\times10^{-3}\omega_o^R t$. The Wigner function, defined as the quasiprobability distribution in phase space

$$W(\alpha)=\frac{2}{\pi}\mathrm{Tr}[\rho D(\alpha)(-1)^{a^\dagger a}D(-\alpha)], \tag{20}$$

where $D(\alpha)=\mathrm{e}^{\alpha a^\dagger-\alpha^* a}$ is the displacement operator for the vibrational mode, with α is the phase-space amplitude. The plane-cut of the Wigner function for the targeted six-phonon state is shown in Fig. 6(a), while that of the ideal six-phonon state is shown in Fig. 6(b). As expected, the Wigner function obtained from prepared state is in well agreement with the result for the ideal six-phonon state.

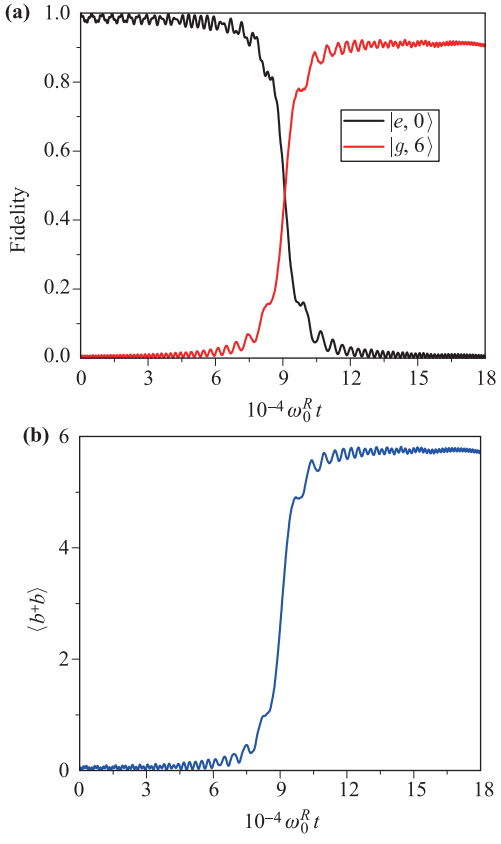

Fig. 5 **(a)** Fidelity of the $|e,0\rangle$ and $|g,6\rangle$ states as a function of gt with the initial state $|e,0\rangle$. **(b)** Expectation value of the photon number $\langle b^\dagger b\rangle$. All results are plotted as functions of $\omega_0^R t$ with $g=0.06\omega_0^R$, $v_c=10^{-6}{\omega_0^R}^2$, $\omega^R=0.168\omega_0^R$, and $\Gamma=\gamma_m=0.0005g$.

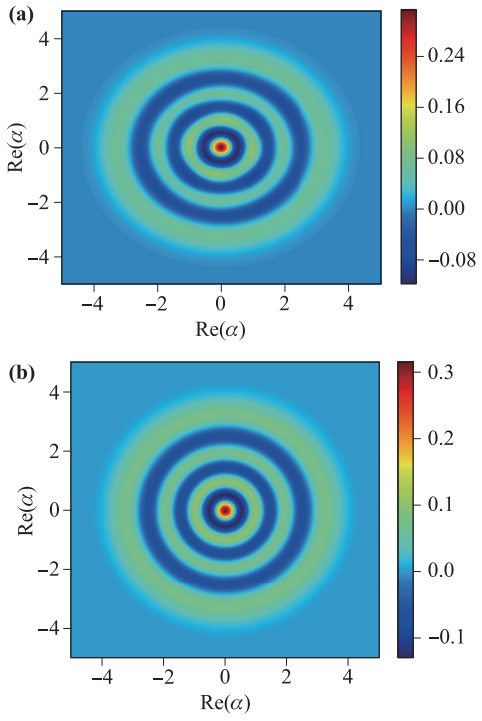

Fig. 6 **(a)** Wigner function along the Re(α) axes for six-phonon state of vibrational modes at the time $gt=1.1\times10^{-3}\omega_o^R t$, which is obtained with the initial state $|e,0\rangle$ by simulating the master equation. The parameters are the same as those in Fig. 5. **(b)** Wigner function along the Re(α) axes for idea six-phonon state.

4 Discussion and conclusions

It is necessary to present a brief discussion of the experimental feasibility of the proposed model. The proposal should work in the single-photon strong-coupling regime, which require the single-photon coupling strength g_0 is much lager than the decay rates of the cavity field γ_c and the mechanical mode γ_m. On the other hand, the two-level approximation of the cavity filed is guaranteed by the photon blockade effect, which requires the nonlinear parameter $\Delta_0=g_0^2/\omega_m$ should be larger than the decay

rate of the cavity field γ_c. According to the current typical experimental parameters, the most promising candidates for realizing our proposal might be the optomechanical crystal devices [79], or the ultracold atoms in optical resonators [80, 81]. However, the parameters used for current experiments still need to be improved for our proposal due to the weak coupling coefficient g_0. Fortunately, a recent report shows that the optomechanical coupling strength can be effectively enhanced to the single-photon strong-coupling regime even when the system is originally in the weak-coupling regime [82]. Another candidate to improve the coupling coefficient is suggested by Pirkkalainen *et al.* [83], where a quantum two-level system (qubit) is added into the optomechanical system, which can effectively increase the coupling strength and allow for rich physics. Thus, with the rapid development of experimental technology, our proposal can be realized in the near future.

In conclusion, we have proposed a scheme to achieve a resonant multi-phonon QRM and adiabatic passage in a cavity mechanical system. In our scheme, the mechanical oscillator is driven by a bichromatic laser which is adjusted to off resonant j-order red- and blue-sideband. In the single-photon strong-coupling regime, the dynamics of this cavity optomechanical system can be treated as a j-phonon resonance quantum Rabi model. Then, we show that such a resonance appears as an avoided crossing of energy curves at the frequency of the simulated bosonic mode is near a fraction of the transition frequency of the simulated two-level system. As a typical example, we theoretically analyze the two-phonon resonance quantum Rabi model, and derive an effective Hamiltonian of the six-phonon coupling. Also, we present a method of six-phonon generation based on adiabatic passage across the resonance. Numerical simulations confirm the validity of the proposed scheme. Finally, with suitable setting the parameters of the driving laser, this method can be extended to the generation of $3j$-phonon state in cavity optomechanical system.

Acknowledgements This work was supported by the National Natural Science Foundation of China under Grant Nos. 11874114, 11674060, 11705030, and 12074070, and the Natural Science Foundation of Fujian Province under Grant No. 2020J01471.

References

1. M. Brune, F. Schmidt-Kaler, A. Maali, J. Dreyer, E. Hagley, J. M. Raimond, and S. Haroche, Quantum Rabi oscillation: A direct test of field quantization in a cavity, *Phys. Rev. Lett.* 76(11), 1800 (1996)
2. Q. Ai, Y. Li, H. Zheng, and C. P. Sun, Quantum anti-Zeno effect without rotating wave approximation, *Phys. Rev. A* 81(4), 042116 (2010)
3. D. Z. Xu, Q. Ai, and C. P. Sun, Dispersive-coupling based quantum Zeno effect in a cavity-QED system, *Phys. Rev. A* 83(2), 022107 (2011)
4. T. Niemczyk, F. Deppe, H. Huebl, E. P. Menzel, F. Hocke, M. J. Schwarz, J. J. Garcia-Ripoll, D. Zueco, T. Hmmer, E. Solano, A. Marx, and R. Gross, Circuit quantum electrodynamics in the ultrastrong-coupling regime, *Nat. Phys.* 6, 772 (2010)
5. P. Forn-Díaz, J. Lisenfeld, D. Marcos, J. J. García-Ripoll, E. Solano, C. J. P. M. Harmans, and J. E. Mooij, Observation of the Bloch–Siegert shift in a qubit-oscillator system in the ultrastrong coupling regime, *Phys. Rev. Lett.* 105(23), 237001 (2010)
6. J. Casanova, G. Romero, I. Lizuain, J. J. García-Ripoll, and E. Solano, Deep strong coupling regime of the Jaynes–Cummings model, *Phys. Rev. Lett.* 105(26), 263603 (2010)
7. S. De Liberato, Light-matter decoupling in the deep strong coupling regime: The breakdown of the Purcell effect, *Phys. Rev. Lett.* 112(1), 016401 (2014)
8. D. Braak, Q. H. Chen, M. T. Batchelor, and E. Solano, Semiclassical and quantum Rabi models: In celebration of 80 years, *J. Phys. A Math. Theor.* 49(30), 300301 (2016)
9. J. F. Huang and C. K. Law, Photon emission via vacuum dressed intermediate states under ultrastrong coupling, *Phys. Rev. A* 89(3), 033827 (2014)
10. L. Garziano, R. Stassi, A. Ridolfo, O. Di Stefano, and S. Savasta, Vacuum-induced symmetry breaking in a superconducting quantum circuit, *Phys. Rev. A* 90(4), 043817 (2014)
11. L. T. Shen, Z. B. Yang, H. Z. Wu, and S. B. Zheng, Quantum phase transition and quench dynamics in the anisotropic Rabi model, *Phys. Rev. A* 95(1), 013819 (2017)
12. S. Ashhab, Superradiance transition in a system with a single qubit and a single oscillator, *Phys. Rev. A* 87(1), 013826 (2013)
13. T. H. Kyaw, S. Felicetti, G. Romero, E. Solano, and L. C. Kwek, Scalable quantum memory in the ultrastrong coupling regime, *Sci. Rep.* 5(1), 8621 (2015)
14. S. Felicetti, E. Rico, C. Sabin, T. Ockenfels, J. Koch, M. Leder, C. Grossert, M. Weitz, and E. Solano, Quantum Rabi model in the Brillouin zone with ultracold atoms, *Phys. Rev. A* 95(1), 013827 (2017)
15. A. Mezzacapo, U. Las Heras, J. S. Pedernales, L. DiCarlo, E. Solano, and L. Lamata, Digital quantum Rabi and Dicke models in superconducting circuits, *Sci. Rep.* 4(1), 7482 (2015)
16. C. H. Alderete and B. M. Rodríguez-Lara, Crosscavity quantum Rabi model, *J. Phys. A Math. Theor.* 49(41), 414001 (2016)
17. R. Puebla, J. Casanova, and M. B. Plenio, A robust scheme for the implementation of the quantum Rabi model in trapped ions, *New J. Phys.* 18(11), 113039 (2016)
18. K. K. W. Ma and C. K. Law, Three-photon resonance and adiabatic passage in the large-detuning Rabi model, *Phys. Rev. A* 92(2), 023842 (2015)
19. L. Garziano, R. Stassi, V. Macrì, A. F. Kockum, S. Savasta, and F. Nori, Multiphoton quantum Rabi oscillations in ultrastrong cavity QED, *Phys. Rev. A* 92(6), 063830 (2015)

20. M. Aspelmeyer, T. J. Kippenberg, and F. Marquardt, Cavity optomechanics, *Rev. Mod. Phys.* 86(4), 1391 (2014)
21. S. Mancini, V. Giovannetti, D. Vitali, and P. Tombesi, Entangling macroscopic oscillators exploiting radiation pressure, *Phys. Rev. Lett.* 88(12), 120401 (2002)
22. X. W. Xu, Y. J. Zhao, and Y. X. Liu, Entangled-state engineering of vibrational modes in a multimembrane optomechanical system, *Phys. Rev. A* 88(2), 022325 (2013)
23. Z. R. Zhong, X. Wang, and W. Qin, Towards quantum entanglement of micromirrors via a two-level atom and radiation pressure, *Front. Phys.* 13(5), 130319 (2018)
24. Y. H. Chen, Z. C. Shi, J. Song, and Y. Xia, Invariantbased inverse engineering for fluctuation transfer between membranes in an optomechanical cavity system, *Phys. Rev. A* 97(2), 023841 (2018)
25. C. S. Hu, Z. Q. Liu, Y. Liu, L. T. Shen, H. Wu, and S. B. Zheng, Entanglement beating in a cavity optomechanical system under two-field driving, *Phys. Rev. A* 101(3), 033810 (2020)
26. S. S. Chen, H. Zhang, Q. Ai, and G. J. Yang, Phononic entanglement concentration via optomechanical interactions, *Phys. Rev. A* 100(5), 052306 (2019)
27. X. B. Yan, H. L. Lu, F. Gao, F. Gao, and L. Yang, Perfect optical nonreciprocity in a double-cavity optomechanical system, *Front. Phys.* 14(5), 52601 (2019)
28. L. Qi, G. L. Wang, S. Liu, S. Zhang, and H. F. Wang, Dissipation-induced topological phase transition and periodic-driving-induced photonic topological state transfer in a small optomechanical lattice, *Front. Phys.* 16(1), 12503 (2021)
29. Z. Zhang, J. Pei, Y. P. Wang, and X. Wang, Measuring orbital angular momentum of vortex beams in optomechanics, *Front. Phys.* 16(3), 32503 (2021)
30. K. Goda, O. Miyakawa, E. E. Mikhailov, S. Saraf, R. Adhikari, K. McKenzie, R. Ward, S. Vass, A. J. Weinstein, and N. Mavalvala, A quantum-enhanced prototype gravitational-wave detector, *Nat. Phys.* 4(6), 472 (2008)
31. U. B. Hoff, G. I. Harris, L. S. Madsen, H. Kerdoncuff, M. Lassen, B. M. Nielsen, W. P. Bowen, and U. L. Andersen, Quantum-enhanced micromechanical displacement sensitivity, *Opt. Lett.* 38(9), 1413 (2013)
32. R. C. Pooser and B. Lawrie, Ultrasensitive measurement of microcantilever displacement below the shotnoise limit, *Optica* 2(5), 393 (2015)
33. C. M. Caves, Quantum-mechanical noise in an interferometer, *Phys. Rev. D* 23(8), 1693 (1981)
34. D. Kienzler, C. Flühmann, V. Negnevitsky, H. Y. Lo, M. Marinelli, D. Nadlinger, and J. P. Home, Observation of quantum interference between separated mechanical oscillator wave packets, *Phys. Rev. Lett.* 116(14), 140402 (2016)
35. J. Q. Liao, Q. Q. Wu, and F. Nori, Entangling two macroscopic mechanical mirrors in a two-cavity optomechanical system, *Phys. Rev. A* 89(1), 014302 (2014)
36. T. Hong, H. Yang, H. Miao, and Y. Chen, Open quantum dynamics of single-photon optomechanical devices, *Phys. Rev. A* 88(2), 023812 (2013)
37. J. Q. Liao, H. K. Cheung, and C. K. Law, Spectrum of single-photon emission and scattering in cavity optomechanics, *Phys. Rev. A* 85(2), 025803 (2012)
38. B. He, Quantum optomechanics beyond linearization, *Phys. Rev. A* 85(6), 063820 (2012)
39. H. Xie, G. W. Lin, X. Chen, Z. H. Chen, and X. M. Lin, Single-photon nonlinearities in a strongly driven optomechanical system with quadratic coupling, *Phys. Rev. A* 93(6), 063860 (2016)
40. X. W. Xu, Y. J. Li, and Y. X. Liu, Photon-induced tunneling in optomechanical systems, *Phys. Rev. A* 87(2), 025803 (2013)
41. A. Kronwald, M. Ludwig, and F. Marquardt, Full photon statistics of a light beam transmitted through an optomechanical system, *Phys. Rev. A* 87(1), 013847 (2013)
42. G. F. Xu and C. K. Law, Dark states of a moving mirror in the single-photon strong-coupling regime, *Phys. Rev. A* 87(5), 053849 (2013)
43. P. Rabl, Photon blockade effect in optomechanical systems, *Phys. Rev. Lett.* 107(6), 063601 (2011)
44. A. Miranowicz, J. Bajer, N. Lambert, Y. X. Liu, and F. Nori, Tunable multiphonon blockade in coupled nanomechanical resonators, *Phys. Rev. A* 93(1), 013808 (2016)
45. A. Miranowicz, J. Bajer, M. Paprzycka, Y. X. Liu, A. M. Zagoskin, and F. Nori, State-dependent photon blockade via quantum-reservoir engineering, *Phys. Rev. A* 90(3), 033831 (2015)
46. V. Macrì, A. Ridolfo, O. Di Stefano, A. F. Kockum, F. Nori, and S. Savasta, Nonperturbative dynamical casimir effect in optomechanical systems: Vacuum Casimir-Rabi splittings, *Phys. Rev. X* 8(1), 011031 (2018)
47. T. Holz, R. Betzholz, and M. Bienert, Suppression of Rabi oscillations in hybrid optomechanical systems, *Phys. Rev. A* 92(4), 043822 (2015)
48. E. Solano, R. L. de Matos Filho, and N. Zagury, Mesoscopic superpositions of vibronic collective states of n trapped ions, *Phys. Rev. Lett.* 87, 060402(4) (2001)
49. P. C. Haljan, K.-A. Brickman, L. Deslauriers, P. J. Lee, and C. Monroe, Spin-dependent forces on trapped ions for phase-stable quantum gates and entangled states of spin and motion, *Phys. Rev. Lett.* 94, 153602(4) (2005)
50. A. Sorensen and K. Molmer, Entanglement and quantum computation with ions in thermal motion, *Phys. Rev. A* 62(2), 022311 (2000)
51. A. Nunnenkamp, K. Børkje, and S. M. Girvin, Single-photon optomechanics, *Phys. Rev. Lett.* 107(6), 063602 (2011)
52. X. H. Cheng, I. Arrazola, J. S. Pedernales, L. Lamata, X. Chen, and E. Solano, Nonlinear quantum Rabi model in trapped ions, *Phys. Rev. A* 97(2), 023624 (2018)
53. R. G. Unanyan, N. V. Vitanov, and K. Bergmann, Preparation of entangled states by adiabatic passage, *Phys. Rev. Lett.* 87(13), 137902 (2001)
54. P. Král, I. Thanopulos, and M. Shapiro, Coherently controlled adiabatic passage, *Rev. Mod. Phys.* 79(1), 53 (2007)
55. M. Weitz, B. C. Young, and S. Chu, Atomic interferometer based on adiabatic population transfer, *Phys. Rev. Lett.* 73(19), 2563 (1994)

56. A. S. Parkins, P. Marte, P. Zoller, and H. J. Kimble, Synthesis of arbitrary quantum states via adiabatic transfer of Zeeman coherence, *Phys. Rev. Lett.* 71(19), 3095 (1993)
57. W. Lange and H. J. Kimble, Dynamic generation of maximally entangled photon multiplets by adiabatic passage, *Phys. Rev. A* 61(6), 063817 (2000)
58. M. Amniat-Talab, S. Lagrange, S. Guérin, and H. R. Jauslin, Generation of multiphoton Fock states by bichromatic adiabatic passage: Topological analysis, *Phys. Rev. A* 70(1), 013807 (2004)
59. S. Y. Ye, Z. R. Zhong, and S. B. Zheng, Deterministic generation of three-dimensional entanglement for two atoms separately trapped in two optical cavities, *Phys. Rev. A* 77(1), 014303 (2007)
60. C. Marr, A. Beige, and G. Rempe, Entangled-state preparation via dissipation-assisted adiabatic passages, *Phys. Rev. A* 68(3), 033817 (2003)
61. K. Toyoda, T. Watanabe, T. Kimura, S. Nomura, S. Haze, and S. Urabe, Generation of Dicke states using adiabatic passage, *Phys. Rev. A* 83(2), 022315 (2011)
62. F. Beaudoin, J. M. Gambetta, and A. Blais, Dissipation and ultrastrong coupling in circuit QED, *Phys. Rev. A* 84(4), 043832 (2011)
63. J. Kabuss, A. Carmele, T. Brandes, and A. Knorr, Optically driven quantum dots as source of coherent cavity phonons: A proposal for a phonon laser scheme, *Phys. Rev. Lett.* 109(5), 054301 (2012)
64. W. Maryam, A. V. Akimov, R. P. Campion, and A. J. Kent, Dynamics of a vertical cavity quantum cascade phonon laser structure, *Nat. Commun.* 4(1), 2184 (2013)
65. H. X. Han, B. W. Li, S. Volz, and Y. A. Kosevich, Ultracompact interference phonon nanocapacitor for storage and lasing of coherent terahertz lattice waves, *Phys. Rev. Lett.* 114(14), 145501 (2015)
66. H. Jing, S. K. Özdemir, X.-Y. Lü, J. Zhang, L. Yang, and F. Nori, *PT*-symmetric phonon laser, *Phys. Rev. Lett.* 113, 053604 (2014)
67. B. He, L. Yang, and M. Xiao, Dynamical phonon laser in coupled active-passive microresonators, *Phys. Rev. A* 109, 054301 (2012)
68. I. S. Grudinin, H. Lee, O. Painter, and K. J. Vahala, Phonon laser action in a tunable two-level system, *Phys. Rev. Lett.* 104(8), 083901 (2010)
69. M. A. Lemonde, S. Meesala, A. Sipahigil, M. J. A. Schuetz, M. D. Lukin, M. Loncar, and P. Rabl, Phonon networks with silicon-vacancy centers in diamond waveguides, *Phys. Rev. Lett.* 120(21), 213603 (2018)
70. G. Calaj' o, M. J. A. Schuetz, H. Pichler, M. D. Lukin, P. Schneeweiss, J. Volz, and P. Rabl, Quantum acoustooptic control of light-matter interactions in nanophotonic networks, *Phys. Rev. A* 99(5), 053852 (2019)
71. M. J. A. Schuetz, E. M. Kessler, G. Giedke, L. M. K. Vandersypen, M. D. Lukin, and J. I. Cirac, Universal quantum transducers based on surface acoustic waves, *Phys. Rev. X* 5(3), 031031 (2015)
72. R. Manenti, A. F. Kockum, A. Patterson, T. Behrle, J. Rahamim, G. Tancredi, F. Nori, and P. J. Leek, Circuit quantum acoustodynamics with surface acoustic waves, *Nat. Commun.* 8(1), 975 (2017)
73. X. Y. Chu, X. Honga, P. Zou, J. Men, and Y. C. Liu, Ultrasensitive protein detection in terms of multiphonon resonance Raman scattering in ZnS nanocrystals, *Appl. Phys. Lett.* 98(25), 253703 (2011)
74. J. J. Viennot, X. Ma, and K. W. Lehnert, Phonon number-sensitive electromechanics, *Phys. Rev. Lett.* 121(18), 183601 (2018)
75. M. Kounalakis, Y. M. Blanter, and G. A. Steele, Synthesizing multi-phonon quantum superposition states using flux-mediated three-body interactions with superconducting qubits, *npj Quant. Inform.* 5, 100, (2019)
76. Y. Chu, P. Kharel, T. Yoon, L. Frunzio, P. T. Rakich, and R. J. Schoelkopf, Creation and control of multi-phonon Fock states in a bulk acoustic-wave resonator, *Nature* 563(7733), 666 (2018)
77. R. Ohira, T. Mukaiyama, and K. Toyoda, Phononnumber-resolving detection of multiple local phonon modes in trapped ions, *Phys. Rev. A* 100, 060301(R) (2019)
78. Q. Bin, X. Y. Lü, F. P. Laussy, F. Nori, and Y. Wu, *N*-phonon bundle emission via the Stokes process, *Phys. Rev. Lett.* 124(5), 053601 (2020)
79. M. Eichenfield, J. Chan, R. M. Camacho, K. J. Vahala, and O. Painter, Optomechanical crystals, *Nature* 462(7269), 78 (2009)
80. J. D. Teufel, T. Donner, D. Li, J. W. Harlow, M. S. Allman, K. Cicak, A. J. Sirois, J. D. Whittaker, K. W. Lehnert, and R. W. Simmonds, Sideband cooling of micromechanical motion to the quantum ground state, *Nature* 475(7356), 359 (2011)
81. S. Gupta, K. L. Moore, K. W. Murch, and D. M. Stamper-Kurn, Cavity nonlinear optics at low photon numbers from collective atomic motion, *Phys. Rev. Lett.* 99(21), 213601 (2007)
82. X. Y. Lü, Y. Wu, J. R. Johansson, H. Jing, J. Zhang, and F. Nori, Squeezed optomechanics with phase-matched amplification and dissipation, *Phys. Rev. Lett.* 114(9), 093602 (2015)
83. J. M. Pirkkalainen, S. U. Cho, F. Massel, J. Tuorila, T. T. Heikkilä, P. J. Hakonen, and M. A. Sillanpää, Cavity optomechanics mediated by a quantum two-level system, *Nat. Commun.* 6(1), 6981 (2015)